Fusion of deterministically generated photonic graph states

Philip Thomas, Leonardo Ruscio, Olivier Morin, and Gerhard Rempe Max-Planck-Institut für Quantenoptik, Hans-Kopfermann-Strasse 1, 85748 Garching, Germany

Entanglement has evolved from an enigmatic concept of quantum physics to a key ingredient of quantum technology. It explains correlations between measurement outcomes that contradict classical physics, and has been widely explored with small sets of individual qubits. Multi-partite entangled states build up in gate-based quantum-computing protocols, and – from a broader perspective – were proposed as the main resource for measurement-based quantum-information processing[1, 2]. The latter requires the ex-ante generation of a multi-qubit entangled state described by a graph[3–6]. Small graph states such as Bell or linear cluster states have been produced with photons[7–16], but the proposed quantum computing and quantum networking applications require fusion of such states into larger and more powerful states in a programmable fashion[17–21]. Here we achieve this goal by employing two individually addressable atoms in one optical resonator[22, 23]. Ring[24] and tree[25] graph states with up to eight qubits, with the names reflecting the entanglement topology, are efficiently fused from the photonic states emitted by the individual atoms. The fusion process itself employs a cavity-assisted gate between the two atoms. Our technique is in principle scalable to even larger numbers of qubits, and is the decisive step towards, for instance, a memory-less quantum repeater in a future quantum internet[26–28].

The characteristics and capabilities of highly entangled graph states [1, 4] have been widely explored in theoretical quantum information science. These states form a useful subclass of multi-partite entangled states and possess the common feature that they can be represented by a graph comprising vertices and edges (Fig. 1a). A variety of quantum information protocols have already been implemented in proofof-principle experiments with graph states made of entangled photons from spontaneous parametric down-conversion (SPDC) sources [8, 29–31]. However, the intrinsically low efficiency of the probabilistic SPDC process remains a severe obstacle for scalability to large qubit numbers. An alternative and in principle deterministic approach using a sequence of single photons emitted from a single memory spin was recognized early on [5, 7, 32] but could not be realized due to technological shortcomings. The strategy was implemented only recently, but with remarkable progress [9–15] that finally led to an out-performance of SPDC systems in the achievable number of entangled photons [16].

While these experiments were limited to elementary photonic graph states such as Greenberger-Horne-Zeilinger (GHZ) and linear cluster states (Fig. 1a), multiple emitter qubits can, in principle, be combined using quantum logic operations to fully leverage their capabilities [17–19, 26, 27]. Once implemented, this would enable architectures that can generate more complex types of graph states for which a plethora of powerful quantum information protocols such as measurement-based quantum computers and quantum repeaters have been proposed [2, 3, 6, 26, 27]. While recent proposals have successfully identified resource-efficient protocols for such architectures [20, 21, 33], the emitters still need to satisfy a number of demanding conditions: a suitable energy level structure for spin-photon entanglement, efficient emission of indistinguishable photons, coherent control of the emitter qubit and high-fidelity entangling gates between emitters. Despite the individual demonstration of these components, no experiment has yet achieved the successful integration of all of them into the same physical system.

Here we demonstrate fusion of photonic graph states produced from two individually addressable atoms in an optical cavity. First, we implement an atom-atom entangling gate based on two-photon interference in the cavity mode [22, 23]. Extending previous work [16], we then show that two graph states separately generated from both emitters can be fused into a larger graph (Fig. 1b). In particular, we demonstrate the generation of two important multi-qubit states, namely ring and tree graph states (see Fig. 1a). Both types of states have been identified as valuable resources for protection against qubit loss and/or computational errors in the framework of measurement-based quantum computation and communication [24–27, 34].

Our experimental setup is schematically shown in Fig. 1d and consists of two ⁸⁷Rb atoms trapped in a high-finesse optical cavity. Both atoms are positioned at anti-nodes of the cavity mode to ensure strong light-matter coupling with a cooperativity of $C \approx 1.6$, and hence to enable efficient generation of single photons via a vacuum-stimulated Raman adiabatic passage (vSTIRAP) [35]. In order to minimize cross-talk between the two emitters, the cavity resonance is detuned by $\Delta = -150 \, \mathrm{MHz}$ with respect to the $|F = 1, m_F = \pm 1\rangle \leftrightarrow$ $|F'=1, m_F=\pm 1\rangle$ transition [36]. Here, we use the atomic state notation $|F, m_F\rangle$, where F(F') denotes the total angular momentum of the ground (excited) state and m_F its projection along the quantization axis. The latter is given by a magnetic field oriented along the y axis (cavity axis), giving rise to a Zeeman splitting with Larmor frequency $\omega_L = 2\pi \times 100 \text{ kHz}.$ The photons are outcoupled from the cavity and directed towards a polarization-resolving detection setup consisting of a polarizing beam splitter and a pair of single-photon detectors. The vSTIRAP control laser can be applied either globally along the x direction acting on both atoms simultaneously or atom-selectively using an acousto-optic deflector (AOD) combined with a high-NA objective on the z axis. Additionally, atomic state manipulation like optical pumping or coher-

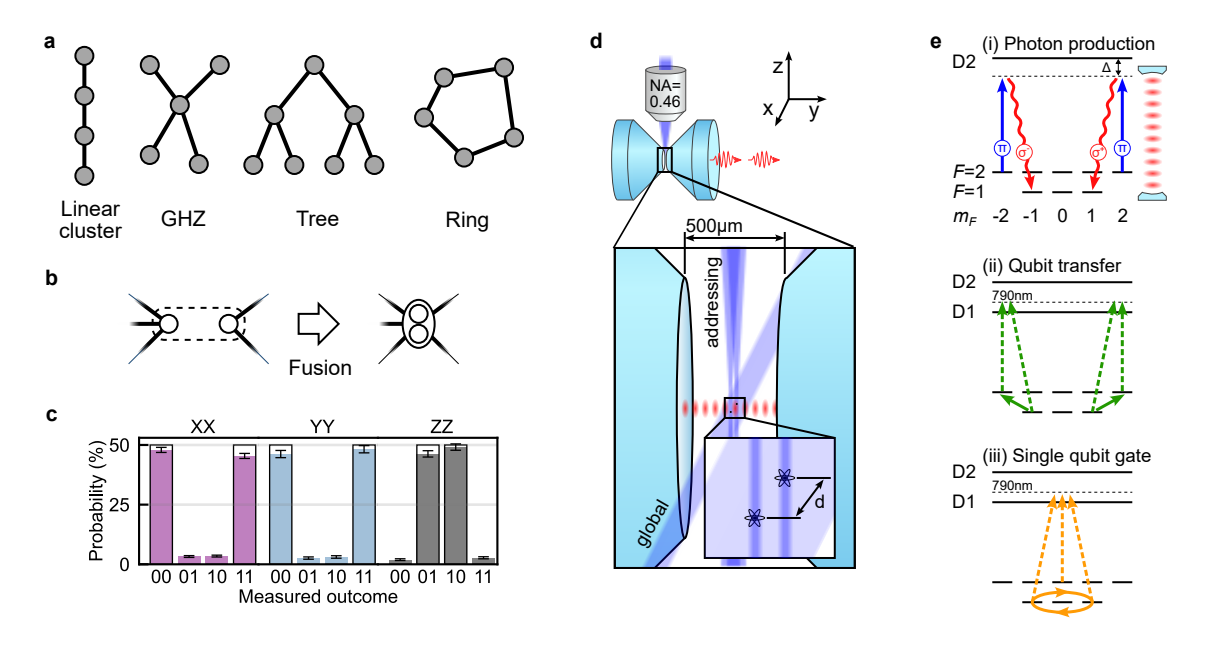


Figure 1. Toolbox for generating photonic graph states. (a) Common examples of graph states. Qubits are represented by vertices, whereas edges connecting them reflect their entanglement topology. (b) Two independent graphs can be merged via a cavity-assisted fusion gate. (c) Correlation measurements on the Bell state $|\psi^+\rangle=(|01\rangle_S+|10\rangle_S)\sqrt{2}$. Correlations in the measurement bases XX,YY and ZZ certify entanglement and good agreement with the ideal $|\psi^+\rangle$ state. Error bars represent the 1σ standard error. (d) Experimental apparatus. Two highly reflective mirrors form an asymmetric high-finesse cavity in which we optically trap two 87 Rb atoms at a distance of $d=9\pm6~\mu m$. The vSTIRAP control laser can be applied either globally or atom-selectively using a high-NA objective. In the process, photons are generated leaving the cavity predominantly via the right mirror. (e) Atomic level scheme illustrating different steps in the protocol. (i) Photon emission from $|2,\pm2\rangle$. (ii) Prior to every photon emission the qubit is mapped from $|1,\pm1\rangle$ to $|2,\pm2\rangle$ using Raman lasers at 790 nm. (iii) The same Raman laser system is used to perform single qubit gates on the qubit states $|1,\pm1\rangle$ (Raman lasers are not shown in panel d).

ent driving of Raman transitions can be carried out on both atoms simultaneously via global laser beams.

Thanks to the single-atom addressing beam, both atoms serve as independent emitters, each capable of generating individual spin-photon entanglement in parallel. An atom residing in a coherent superposition of the states $|2,\pm 2\rangle$ can undergo a two-photon transition (vSTIRAP) to $|1,\pm 1\rangle$ emitting a photon into the cavity mode (see Fig. 1e (i)). We choose the states $|0\rangle_S \equiv |1,+1\rangle$ and $|1\rangle_S \equiv |1,-1\rangle$ as the atomic qubit basis ('S' for 'spin'). In the emission process, conservation of angular momentum gives rise to entanglement between the polarization of the photon and the atomic spin state. $|0\rangle \equiv |R\rangle$ and $|1\rangle \equiv |L\rangle$ define the photonic qubit, with R/L corresponding to right/left circular polarization, respectively. This process can be repeated after a Raman transfer from $|1,\pm 1\rangle$ back to $|2,\pm 2\rangle$. Using a specifically designed alternating sequence of photon emissions and atomic qubit rotations, elementary graph states such as GHZ or linear cluster states can be obtained [16].

The global beam provides the possibility to entangle the two emitters, thus merging the graphs they are connected to. The underlying mechanism involves two-photon interference in the cavity mode and resembles the Type-II fusion gate [37]. Although not strictly identical to fusion in its original form, we here refer to our implementation as a 'cavity-assisted fusion gate'. The quality of this process crucially depends on the

indistinguishability of the photons, which is ensured here by both atoms coupling to the same cavity mode and vSTIRAP control laser. In order to quantitatively characterize this process, we use the cavity-assisted fusion gate to entangle the two atoms and analyze the correlations in the obtained two-qubit state. To this end, we initialize both atoms by optical pumping to the state $|2,0\rangle$. Next, we carry out the fusion by applying a global vSTIRAP control pulse generating two entangled spin-photon pairs. As the photons interfere in the cavity mode, the which-atom information is erased. Therefore, subsequent measurement in the $Z\left(R/L\right)$ basis, with one photon being detected in each detector, projects the atoms onto the Bell state $|\psi^+\rangle = (|01\rangle_S + |10\rangle_S)/\sqrt{2}$ and heralds the success of the entangling operation.

We observe strong correlations when measuring the atoms in the bases XX,YY and ZZ (Methods). The probability of each measurement outcome in the different bases is plotted in Fig. 1c. From this we obtain a state fidelity $\mathcal{F}=0.915(5)$ w.r.t. the ideal state. This number varies between 0.851(6) and 0.963(8) depending on the choice of post-selection criteria for the photon arrival times (Methods). The scenario described above is the simplest case of the fusion mechanism depicted in Fig. 1b, in which the emitter qubits do not share a bond with any other qubit prior to the fusion. The resulting state $|\psi^+\rangle$ can be interpreted as a logical qubit redundantly encoded [19,37] in the basis $\{|0\rangle_L \equiv |10\rangle_S, |1\rangle_L \equiv |01\rangle_S\}$

('L' for logic). In the graph state picture we express this as a vertex containing two circles. As we will see below, the same principle applies when the two atoms are part of a graph state and do share bonds with other qubits. In this case the two emitter vertices are merged, preserving the bonds attached to them as shown in Fig. 1b.

We now use the two-atom Bell pair as a starting point for preparing various photonic graph states. As a first example we demonstrate the generation of ring graph states consisting of up to eight qubits (Fig. 2e). In essence, we first grow a linear cluster state with the emitters at the ends of the chain, which we then fuse to obtain a ring. The generation steps are depicted in Fig. 2a using the graph state representation. We start with a two-atom Bell state $|\psi^+\rangle$ which we obtain from the cavity-assisted fusion. Next, we apply N photongeneration cycles interleaved with $\pi/2$ pulses resulting in a linear cluster state with the atoms at its ends. Within a given cycle the photon generation from both atoms is separated by $T \approx 20 \,\mu \text{s}$. In the final step we perform the fusion on the emitter qubits in order to merge both ends of the chain. For N=2 and N=3 photon generation cycles this produces either a box- or hexagon-shaped graph as shown in Fig. 2b and e, respectively. Here again, the two atoms carry a logical qubit redundantly encoded in $|10\rangle_S$ and $|01\rangle_S$. This specific protocol only produces ring graph states of even parity, i.e. an even number of vertices. However, as we show in the Methods, ring graph states of odd parity can be obtained simply by adding a global $\pi/4$ rotation after the initial fusion gate. In the following, we will focus on the protocol as presented above and demonstrate the generation of the box and hexagon graphs, consisting of four and six vertices, respectively.

In order to characterize the experimentally generated state and compare it with the ideal graph state, we measure its corresponding stabilizer operators. The stabilizers to a given graph are defined as $S_i = X_i \prod_{j \in \mathcal{N}_i} Z_j$, where \mathcal{N}_i is the neighborhood of vertex i. As the cavity-assisted fusion gate produces vertices that are encoded by two physical qubits, we use the concept of 'redundantly-encoded graph states' [19]. These are equivalent to regular graph states up to a local unitary transformation on the redundant physical qubits. The stabilizers to the graphs in Fig. 2b and E are displayed on the x axis of Fig. 2c and f. To obtain the expectation value of a given stabilizer, we measure coincidences of the corresponding subset of qubits, where each qubit is detected either in the Z or X basis. For photonic qubits the detection basis is set dvnamically via an electro-optic polarization modulator (EOM). The readout of the atomic qubit is realized by an appropriate Raman rotation to set the basis, followed by up to three photon generation attempts with the detection basis set to R/L(Methods).

The experimentally measured expectation values of the stabilizers are displayed in Fig. 2c and f for the box and hexagon graphs, respectively. Furthermore, in the case of an even number of vertices, it is possible to divide the stabilizers into two sets a and b, which can be measured with two local measurement settings M_a and M_b . Similar to Tóth $et\ al.$ [38], we in-

troduce the operators G_a , G_b and $P=G_a+G_b-1$, which define the fidelity lower bound $\mathcal{F} \geq \langle P \rangle$. $G_{a/b}$ is simply the product $\prod_{i \in a/b} (1+S_i)/2$ obtained from the measurement setting $M_{a/b}$ (Methods).

The results are shown in Fig. 2 d and g. For the box-shaped graph we find the fidelity to be lower bounded by 0.59(3), surpassing the threshold of 0.5 and thereby certifying genuine multi-partite entanglement. In the case of the hexagon graph, the data do not prove genuine entanglement as $\langle P \rangle = 0.34^{+0.06}_{-0.07}$. We nonetheless observe an overlap with the ideal graph state in terms of the stabilizer expectation values $\langle S_i \rangle$. Moreover, we emphasize that the true state fidelity is likely to be higher than the obtained lower bound $\langle P \rangle$. Alternative characterization methods have been developed for a more precise estimation of the fidelity [39, 40], but are unsuitable for our current detection setup.

As a second example we demonstrate the generation of a tree graph state [25] consisting of eight qubits (Fig. 3c). In this scenario we fuse two independent graphs into a larger one. To do so, we first generate two GHZ states, each represented by a star-shaped graph. These will eventually form two branches of the tree graph after merging them via the cavity-assisted fusion gate. The experimental protocol is depicted in Fig. 3a. After initialization to the $|2,0\rangle$ state, each atom emits a photon upon successively sending the vSTIRAP control pulse onto the atoms via the addressing system, generating two atom-photon entangled pairs (Fig. 3a, (1)). Two further photon production cycles are carried out, each cycle consisting of a global Raman transfer to $|2,\pm 2\rangle$ and a photon generation pulse (Fig. 3a, (2,3)). Next, after a free evolution time of t_0 , a $\pi/2$ rotation is applied to both atomic qubits simultaneously. At this stage two GHZ states of the form

$$(|+\rangle_S |0++\rangle + e^{i\phi(t_0)} |-\rangle_S |1--\rangle)/\sqrt{2}$$
 (1)

have been generated, each consisting of one atom and three photons. Here $|\pm\rangle=(|0\rangle\pm|1\rangle)/\sqrt{2}$. Note that two of the photons in the above expression have experienced a Hadamard rotation, which in the experiment is absorbed into the setting of the measurement basis. This as well as a $\pi/2$ pulse on the atomic qubit has the effect that the respective qubit is 'pushed out' from the graph, thus forming a so-called 'leaf' qubit (see, e.g. [19]).

The second term in Eq. 1 above carries a phase factor $\phi(t_0)$ which arises from the free evolution of the atomic qubit. It depends on the timing of the $\pi/2$ pulse given by the parameter t_0 . Fig. 3b displays the parity of each of the GHZ states and the oscillating behavior as a function of t_0 . We show that by adjusting t_0 and the temporal photon separation T we can actively tune this phase to be 0 and π for the two branches, respectively.

In the next step the two branches are fused into a tree graph. To do so, we apply a global vSTIRAP control pulse leading to the simultaneous emission of two photons which are detected in the R/L basis. As before, the protocol succeeds if one photon is detected in each detector, i.e. in the R and L polarization states, respectively. This step can be thought of as a pro-

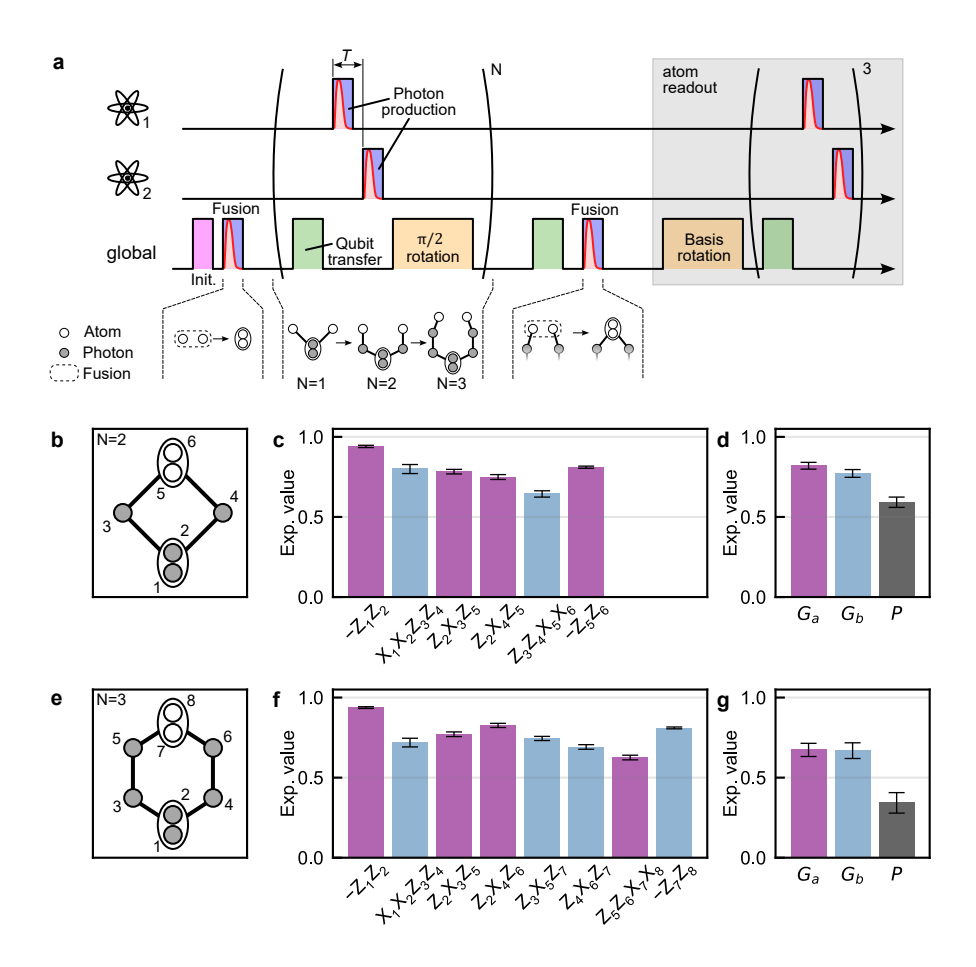


Figure 2. **Ring graph states.** (a) Experimental protocol showing the individual steps such as initialization (purple), vSTIRAP control pulse (blue), photons (red), qubit transfer (green), qubit rotation (orange). The color coding follows Fig. 1e. Each of the three lines represents operations carried out on atom 1, atom 2 or globally, i.e. via a global laser beam acting on both atoms simultaneously. The multi-qubit quantum state is shown below in its graph representation at different stages of the sequence. (b/e) Graph representation of the generated 'box' and 'hexagon' graph states. (c/f) Measured expectation values for the stabilizers corresponding to the box/hexagon-shaped graphs in (b/e). The color of the bars (purple and blue) identifies the two sets of stabilizers a and b corresponding to the measurement settings a and b correlators a and b and b and b and b and fidelity lower bound b in black. All error bars represent the a standard error.

jection of the atomic qubits on the subspace $\{|01\rangle_S\,, |10\rangle_S\},$ given by the operator $|01\rangle_S\,\langle 01|_S + |10\rangle_S\,\langle 10|_S.$ We then obtain the state

$$|\psi_{tree}\rangle = \frac{1}{2\sqrt{2}} \Big(|10\rangle_S (|0++\rangle + |1--\rangle)^{\otimes 2} + |01\rangle_S (|0++\rangle - |1--\rangle)^{\otimes 2} \Big),$$
(2)

which is an eigenstate to a set of stabilizers corresponding to a tree graph state of depth two, where the root qubit can be seen as redundantly encoded (Fig. 3c). Due to the redundant encoding, we again use the modified stabilizers $S_1 = -Z_1Z_2$ and $S_2 = X_1X_2Z_3Z_6$ for the physical qubits of the root vertex.

The measured expectation values for the stabilizers are displayed in Fig. 3d. We find all stabilizers to be above 0.7 and some of them close to one, certifying a good agreement with the ideal state for which $\langle S_i \rangle = 1$. Furthermore, we are able to prove genuine multi-partite entanglement by collecting 8-

qubit coincidences. We find that the entanglement fidelity exceeds the classical threshold of 0.5 with $\mathcal{F} \geq 0.69^{+0.04}_{-0.05}$.

The generation of the presented graph states relies on a high overall source-to-detector efficiency, which in this work is close to 0.5 for a single photon emission. Hence, with a coincidence rate on the order of one per minute, we can collect hundreds of events within a few hours of measurement (Methods).

In conclusion, we have generated ring graph states of up to 6 (8) logical (physical) qubits and a tree graph state made up of 7 (8) logical (physical) qubits by coupling two emitters via a cavity-assisted fusion gate. The latter constitutes the, in our view, decisive step towards scalable architectures of coupled single-photon sources for creating arbitrary photonic graph states. For instance, a larger number of emitters either in the same or in spatially separated cavities would enable tree states of higher depths or repeater graph states which are proposed as useful tools to overcome photon loss in long-

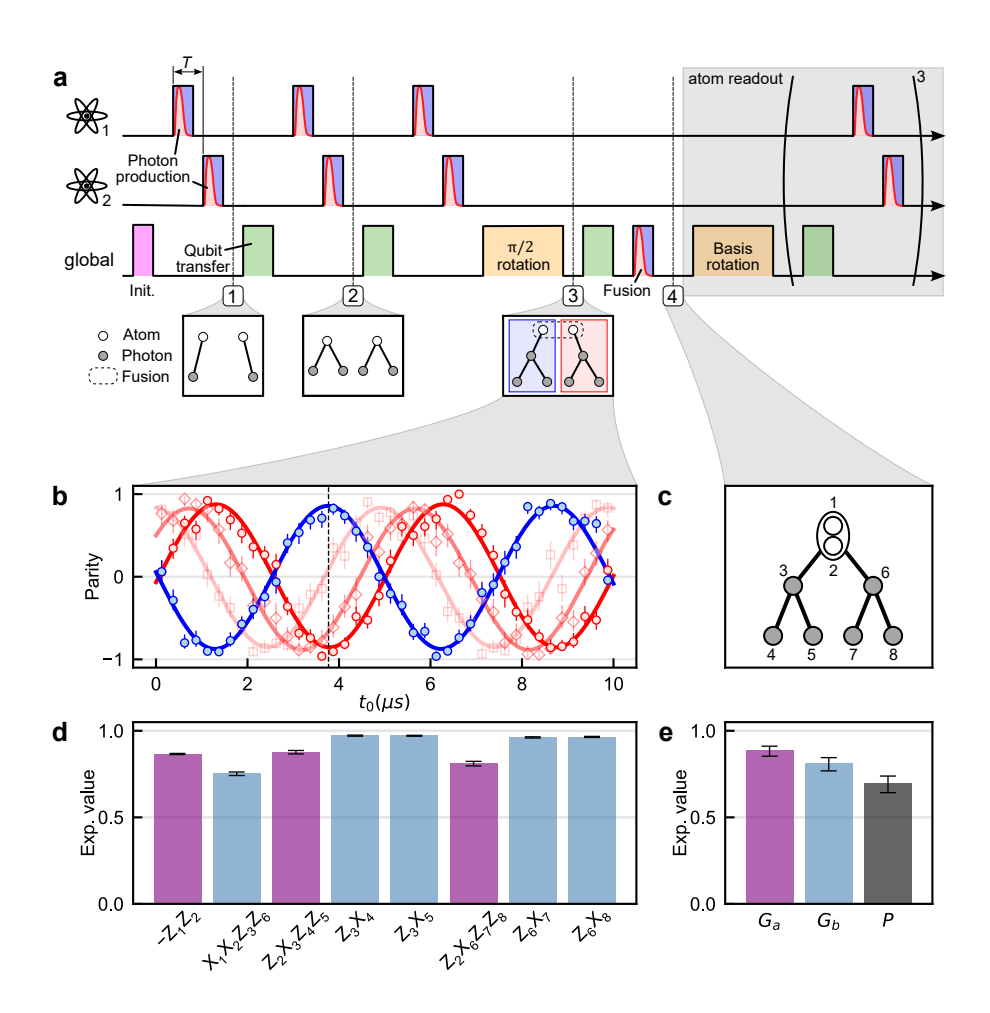


Figure 3. Tree graph states. (a) Experimental protocol similar to Fig. 2a. (b) Quantum phase synchronization between the two branches of the tree. The data show the parity of each four-qubit GHZ state as a function of free evolution time t_0 before the $\pi/2$ rotation. The parity of both branches is tuned to give a relative π phase difference. The dashed vertical line indicates the working point used for the experiment. Data in light red displays the parity when slightly varying the photon separation T (see main text). (c) Graph representation of the generated multi-qubit state with the chosen labeling convention. (d) Measured stabilizer expectation values similar to Fig. 2. (e) Product correlators G_a (purple) and G_b (blue) and fidelity lower bound P (black). All error bars represent the 1σ standard error.

distance transmission lines [6, 26, 27]. Similar schemes can be employed to generate two-dimensional cluster states to enable fault-tolerant quantum computing protocols such as one-way or fusion-based quantum computation [2, 24, 34]. Finally yet importantly, the photons of the graph state could be individually steered to and stored in a distributed set of heralded quantum memories [41], thereby bringing the flying entanglement to a standstill in a material system. In the context of multi-partite quantum networks [42] this approach would offer a plethora of fascinating possibilities [28] beyond those of a two-party quantum-communication link.

ACKNOWLEDGMENTS

P.T. thanks G. Styliaris for valuable discussions. This work was supported by the Bundesministerium für Bildung und Forschung via the Verbund QR.X (16KISQ019), by the Deutsche Forschungsgemeinschaft under Germany's Excel-

lence Strategy – EXC-2111 – 390814868, and by the European Union's Horizon Europe research and innovation program via the project QIA-Phase 1 under grant agreement No. 101102140. The opinions expressed in this document reflect only the authors' view and reflects in no way the European Commission's opinions. The European Commission is not responsible for any use that may be made of the information it contains.

^[1] Briegel, H. J. and Raussendorf, R., Persistent entanglement in arrays of interacting particles. Phys. Rev. Lett. **86**, 910 (2001).

^[2] Raussendorf, R. and Briegel, H. J., A One-Way Quantum Computer, Phys. Rev. Lett. 86, 5188 (2001)

^[3] Barrett, S. D. and Kok, P., Efficient high-fidelity quantum computation using matter qubits and linear optics. Phys. Rev. A 71, 060310(R) (2005).

- [4] Hein, M., Dür, W., Eisert, J., Raussendorf, R., Van den Nest, M. and Briegel, H. J. in *Quantum Computers, Algorithms and Chaos*. Vol. 162 Proceedings of the International School of Physics "Enrico Fermi" 115-218 (IOS Press, 2006).
- [5] Lindner, N. H., and Rudolph, T., Proposal for Pulsed On-Demand Sources of Photonic Cluster State Strings. Phys. Rev. Lett. 103, 113602 (2009).
- [6] Azuma, K., Tamaki, K. and Lo, H.-K., All-photonic quantum repeaters. Nat. Commun. 6, 6787 (2015).
- [7] Wilk, T., Webster, S. C., Kuhn, A. and Rempe, G., Single-Atom Single-Photon Quantum Interface. Science 317, 488-490 (2007).
- [8] Walther, P. et al. Experimental one-way quantum computing. Nature 434, 169–176 (2005).
- [9] Schwartz, I. et al. Deterministic generation of a cluster state of entangled photons. Science 354, 434-437 (2016).
- [10] Istrati, D. et al. Sequential generation of linear cluster statesfrom a single photon emitter. Nat. Commun. 11, 5501 (2020).
- [11] Besse, J.-C. et al. Realizing a deterministic source of multipartite-entangled photonic qubits. Nat. Commun. 11, 4877 (2020)
- [12] Yang, C. W., Yu, Y., Li, J., Bao, X.-H. and Pan, J.-W., Sequential generation of multiphoton entanglement with a Rydberg superatom. Nat. Phot. 16, 658–661 (2022).
- [13] Ferreira, V. S., Kim, G., Butler, A., Pichler, H. and Painter, O., Deterministic generation of multidimensional photonic cluster states with a single quantum emitter. Nat. Phys. (2024).
- [14] Cogan, D., Su, Z.-E., Kenneth, O. and Gershoni, D., Deterministic generation of indistinguishable photons in a cluster state. Nat. Photon. 17, 324–329 (2023).
- [15] Coste, N. et al. High-rate entanglement between a semiconductor spin and indistinguishable photons. Nat. Photon. 17, 582–587 (2023).
- [16] Thomas, P., Ruscio, L., Morin, O. and Rempe, G., Efficient generation of entangled multiphoton graph states from a single atom. Nature 608, 677–681 (2022).
- [17] Economou, S. E., Lindner, N. and Rudolph, T., Optically generated 2-dimensional photonic cluster state from coupled quantum dots. Phys. Rev. Lett. 105, 093601 (2010).
- [18] Russo, A., Barnes, E. and Economou, S. E., Generation of arbitrary all-photonic graph states from quantum emitters. New J. Phys. 21, 055002 (2019).
- [19] Hilaire, P., Vidro, L., Eisenberg, H. S. and Economou, S. E., Near-deterministic hybrid generation of arbitrary photonic graph states using a single quantum emitter and linear optics. Ouantum 7, 992 (2023).
- [20] Li, B., Economou, S. E. and Barnes, E., Photonic resource state generation from a minimal number of quantum emitters. npj Quantum Inf 8, 11 (2022).
- [21] Löbl, M. C., Paesani, S. and Sørensen, A. S., Loss-tolerant architecture for quantum computing with quantum emitters. preprint arXiv:2304.03796v1 (2023).
- [22] Casabone, B. et al., Heralded entanglement of two ions in an optical cavity. Phys. Rev. Lett. 111, 100505 (2013).
- [23] Langenfeld, S., Thomas, P., Morin, O. and Rempe, G., Quantum Repeater Node Demonstrating Unconditionally Secure Key Distribution. Phys. Rev. Lett. 126, 230506 (2021).
- [24] Bartolucci, S. et al., Fusion-based quantum computation. Nat. Commun. 14, 912 (2023).
- [25] Varnava, M., Browne, D. E. and Rudolph, T., Loss Tolerance in One-Way Quantum Computation via Counterfactual Error Correction. Phys. Rev. Lett. 97, 120501 (2006).
- [26] Buterakos, D., Barnes, E., and Economou, S. E., Deterministic generation of all-photonic quantum repeaters from solid-state

- emitters. Phys. Rev. X 7, 041023 (2017).
- [27] Borregaard, J. et al. One-way quantum repeater based on near-deterministic photon-emitter interfaces. Phys. Rev. X 10, 021071 (2020).
- [28] Epping, M., Kampermann, H. and Bruß, D., Large-scale quantum networks based on graphs. New J. Phys. 18, 053036 (2016)
- [29] Yao, X.-C. et al. Experimental demonstration of topological error correction. Nature 482, 489–494 (2012).
- [30] Bell, B. A. et al. Experimental demonstration of a graph state quantum error-correction code. Nat. Commun. 5, 3658 (2014).
- [31] Zhong, H.-S. et al. 12-Photon Entanglement and Scalable Scattershot Boson Sampling with Optimal Entangled-Photon Pairs from Parametric Down-Conversion, Phys. Rev. Lett. 121, 250505 (2018)
- [32] Schön, C., Solano, E., Verstraete, F., Cirac and J. I., Wolf, M. M., Sequential generation of entangled multiqubit states. Phys. Rev. Lett. 95, 110503 (2005).
- [33] Zilk, F. et al., A compiler for universal photonic quantum computers. 2022 IEEE/ACM Third International Workshop on Quantum Computing Software (QCS), Dallas, TX, USA, 2022, pp. 57-67
- [34] Bell, T. J., Pettersson, L. A. and Paesani, S., Optimizing Graph Codes for Measurement-Based Loss Tolerance. PRX Quantum 4, 020328 (2023).
- [35] Morin, O., Körber, M., Langenfeld, S. and Rempe, G., Deterministic shaping and reshaping of single-photon temporal wave functions. Phys. Rev. Lett. 123, 133602 (2019).
- [36] Langenfeld, S., Morin, O., Körber, M. and Rempe, G., A network-ready random-access qubits memory. npj Quantum Inf 6, 86 (2020).
- [37] Browne, D. E. and Rudolph, T., Resource-efficient linear optical quantum computation. Phys. Rev. Lett. 95, 010501 (2005).
- [38] Tóth, G. and Gühne, O., Detecting Genuine Multipartite Entanglement with Two Local Measurements. Phys. Rev. Lett. 94, 060501 (2005).
- [39] Flammia, S. T. and Liu, Y.-K., Direct Fidelity Estimation from Few Pauli Measurements. Phys. Rev. Lett. 106, 230501 (2011)
- [40] Tiurev, K. and Sørensen, A. S., Fidelity measurement of a multiqubit cluster state with minimal effort. Phys. Rev. Research 4, 033162 (2022)
- [41] Brekenfeld, M., Niemietz, D., Christesen, J.D. and Rempe, G., A quantum network node with crossed optical fibre cavities. Nat. Phys. 16, 647–651 (2020).
- [42] Pompili, M. et al. Realization of a multinode quantum network of remote solid-state qubits. Science 372, 259-264 (2021).

METHODS

Experimental setup

The apparatus used in our work consists of a single-sided high-finesse cavity in which we optically trap two Rubidium atoms. Most experimental details about the setup including the cavity QED parameters have already been described elsewhere [16]. In the following we provide further information which is important for the current work.

The atoms are trapped in a two-dimensional optical standing-wave potential formed by two pairs of counter-propagating laser beams. The first is a retro-reflected laser at a wavelength of $\lambda=1064~\mathrm{nm}$ along the x axis. The second one propagates inside the cavity mode along the y axis with $\lambda=772~\mathrm{nm}$. The atoms are loaded from a magneto optical trap (MOT) to the cavity center via a second $1064~\mathrm{nm}$ running wave laser. The light scattered by the atom during laser cooling is imaged via the objective onto an EMCCD (electron-multiplying charge-coupled device) camera in order to spatially resolve the position of the atoms. After each loading attempt we find a random number of atoms n at random positions. The experimental control software identifies atom pairs with a suitable relative distance d. If no such atom pair is present, a new loading attempt starts immediately. Otherwise, a tightly-focused resonant laser beam, propagating through the objective and steered by the AOD, removes the n-2 unwanted atoms. The x component of the center-of-mass position of the atom pair $(x_2+x_1)/2$ is then actively stabilized to the center of the cavity mode by acting on the relative phase of the $1064~\mathrm{nm}$ counter-propagating laser beams. The y components y_1 and y_2 are controlled by modulating the optical power of the $772~\mathrm{nm}$ intra-cavity trap until the atoms are found in a desired position.

Fusion gate and post-selection

For a fusion gate to be successful, two photons have to be detected as described in the main text. Due to imperfections in the emission process the absolute arrival time as well as the relative time difference between the two photons can have an effect on the fidelity. Sources of imperfections are mainly spontaneous scattering via the excited state and non-perfect temporal mode overlap of the two photons. The influence of the arrival time on the fidelity of the atom-atom Bell state is summarized in Extended Data Fig. 1. Panel a shows the intensity profile of the photon temporal wave function as a function of $t_{R,L}$, with t_R and t_L being the arrival time of the R and L polarized photons produced in the fusion process, respectively. Events in which a photon arrives outside the time interval marked by the dashed lines are discarded. This interval contains about 98% of all single-photon counts. Panel b is a two-dimensional density plot of the number of two-photon events versus arrival times t_R and t_L . One can see that most events lie in the vicinity of the point $t_R = t_L = 200$ ns. The dashed line encloses the region defining the post-selection criteria which we specify in more detail below. Panel c is a density plot similar to b displaying the fidelity as a function of t_R and t_L . We find that the fidelity is highest near the diagonal of the plot, that is $t_R \approx t_L$. This motivates our choice of the post-selection region enclosed by the dashed line. Pixels for which we did not acquire enough data to compute the fidelity are shown in white. The fidelity is computed using the formula

$$\mathcal{F} = \frac{1}{4} \left(1 + \langle XX \rangle + \langle YY \rangle - \langle ZZ \rangle \right). \tag{3}$$

Here XX, YY and ZZ are two-qubit operators consisting of the respective Pauli operators. In panels (d-f) we analyze their expectation values $\langle XX \rangle$, $\langle YY \rangle$ and $\langle ZZ \rangle$ as a function of arrival time difference $|t_R - t_L|$. We plot the expectation value both for $|t_R - t_L| = \tau$ (orange) and $|t_R - t_L| \leq \tau$ (purple), e.g. the cumulative expectation value. We find all correlators to be in good agreement with the ideal case, for which we expect $\langle XX \rangle = \langle YY \rangle = 1$ and $\langle ZZ \rangle = -1$. The high fidelity of the two-atom Bell state is also an indicator of a high photon-indistinguishability. The dashed lines mark the maximum value of τ , i.e. $|t_R - t_L| \leq \tau$, chosen for the data presented in Fig. 1c of the main text.

Post-selection criteria

For the data in Extended Data Fig. 1c, we apply two post-selection steps. The first step consists of restricting the absolute detection time of the photons to a predefined interval of $1~\mu s$ width (see dashed lines in Extended Data Fig. 1 panel a). The second post-selection condition involves the relative arrival time difference $|t_R-t_L|$ in the case of two-photon events. The diagonal dashed lines in Extended Data Fig. 1 b and c mark the condition $|t_R-t_L| \leq \tau_{max} = 250~\mathrm{ns}$. Events in which the photons are detected with a relative delay larger than τ_{max} are discarded. In about 80% of experimental runs the two photon fall within the interval of τ_{max} .

As stated in the main text the atom-atom Bell state fidelity ranges between 0.851(6) and 0.963(8). The first number refers to the scenario where no post-selection on the photon arrival time is applied. The second number is obtained when restricting the photon arrival times to $t_{R,L} \le 500$ ns and $|t_R - t_L| \le 20$ ns. In this case the post-selection ratio is about 15%.

The above numbers refer to the scenario in which the atom is initialized to $|F=2,m_F=0\rangle$ prior to photon generation. However, in the ring and tree state protocol, most photons are generated from $|F=2,m_F=\pm 2\rangle$. In this case, the photon wavepacket is slightly longer as the $m_F=\pm 2$ Zeeman sublevels couple to different excited states in the emission process. We here apply the same $1~\mu s$ time interval as for the $m_F=0$ case, as at least 95% of the photon wavepacket is enclosed by this window. However, for the two-photon events in the fusion process we choose a maximum time difference of $\tau_{max}=400~\mathrm{ns}$ to accommodate for a post-selection fraction of about 80%, similar to the $m_F=0$ case.

Atom readout

At the end of the generation sequence for tree and ring graph states the atomic qubits are still entangled with the photons previously generated. One way to measure the atomic qubits is to perform an atom-to-photon state transfer as done in ref. [16]. Here, the qubit is mapped from $|F=1,m_F\pm1\rangle$ to $|F=2,m_F=\pm1\rangle$ prior to photon production. In this way, the qubit is fully transferred to the photon which can then be measured optically. In this work, however, we chose another technique to measure the atomic qubit. For a Z measurement we transfer the qubit to $|F=2,m_F=\pm2\rangle$ and generate a photon measuring it in the R/L basis. Detecting an R (L) photon projects the atomic qubit onto the state $|0\rangle_S$ ($|1\rangle_S$). When measuring the qubit in X or Y, we set the basis directly on the atomic qubit with a $\pi/2$ pulse whose phase is tuned according to the basis. The advantage of this scheme is that it can be repeated until success in the case of photon loss, thus increasing the overall efficiency of the state readout. However, as errors are more likely to occur after many repetitions, we limit the number of attempts to three.

Detailed protocol description

In the following, we will describe the generation protocol for the ring and tree graph states with explicit expressions for each step. In the derivation we do not explicitly include the free evolution of the atomic qubit. In the experiment the phases that arise from the qubit oscillation are tracked by measuring the stabilizer operators as a function of certain timing parameters related to, for instance, Raman transfers and photon emissions. Importantly, these phases may be tuned for each atom independently by varying the respective time of the photon production pulse.

Ring states

We first describe the protocol of the ring graph states and choose the pentagon ring as a specific example. The box- and hexagon-shaped graphs are obtained from a similar protocol, only omitting a single $\pi/4$ rotation. A sketch of the experimental sequence is given in Extended Data Fig. 2, panel a.

The first step of the protocol is to entangle the two atoms and prepare them in the Bell state $|\psi^{+}\rangle = (|01\rangle_S + |10\rangle_S)/\sqrt{2}$. In order to obtain the pentagon graph, which has an odd number of vertices, we here need to apply a global $-\pi/4$ pulse. This 'pushes' the two qubits apart, forming two separate vertices with an edge between them (Extended Data Fig. 2,a(2)). The corresponding state (omitting normalization constants) reads

$$\frac{-\pi/4}{\longrightarrow} |00\rangle_S + |01\rangle_S + |10\rangle_S - |11\rangle_S$$

$$= |0+\rangle_S + |1-\rangle_S .$$
(4)

Here we have substituted the transformations

$$|0\rangle_S \xrightarrow{-\pi/4} \cos\left(\frac{\theta}{2}\right)|0\rangle_S + \sin\left(\frac{\theta}{2}\right)|1\rangle_S ,$$
 (5)

$$|1\rangle_S \xrightarrow{-\pi/4} -\sin\left(\frac{\theta}{2}\right)|0\rangle_S + \cos\left(\frac{\theta}{2}\right)|1\rangle_S ,$$
 (6)

and used $\theta = -\pi/4$ as well as $\cos\left(\frac{\pi}{8}\right) = \frac{\sqrt{2+\sqrt{2}}}{2}$ and $\sin\left(\frac{\pi}{8}\right) = \frac{\sqrt{2-\sqrt{2}}}{2}$. Subsequently, each atom emits a photon, giving

$$\xrightarrow{PP} |0\rangle |0\rangle (|0\rangle + |1\rangle |1\rangle) + |1\rangle |1\rangle (|0\rangle |0\rangle_S - |1\rangle |1\rangle_S), \tag{7}$$

followed by a $\pi/2$ rotation on the atomic qubits:

$$\frac{\pi/2}{\langle |+\rangle_S |0\rangle + |-\rangle_S |1\rangle \rangle |0\rangle |+\rangle_S + \langle |+\rangle_S |0\rangle - |-\rangle_S |1\rangle \rangle |1\rangle |-\rangle_S
= (|0\rangle_S |+\rangle + |1\rangle_S |-\rangle) |0\rangle |+\rangle_S + (|0\rangle_S |-\rangle + |1\rangle_S |+\rangle) |1\rangle |-\rangle_S ,$$
(8)

which is equal to a 4-qubit linear cluster state with the atoms at both ends of the chain. Note that the (global) $\pi/2$ pulse affects only the spin component of the multi-qubit state. We perform another photon production on both spins

$$\xrightarrow{PP} (|0\rangle_S |0+\rangle + |1\rangle_S |1-\rangle) |0\rangle (|0\rangle |0\rangle_S + |1\rangle |1\rangle_S)
+ (|0\rangle_S |0-\rangle + |1\rangle_S |1+\rangle) |1\rangle (|0\rangle |0\rangle_S - |1\rangle |1\rangle_S).$$
(9)

We apply a Z gate to qubit 6 and a Hadamard to qubit 1 and 6 (indices run from left to right).

$$\frac{H_1 \otimes Z_6 \otimes H_6}{\langle (|+\rangle_S |0+\rangle + |-\rangle_S |1-\rangle) |0\rangle (|-\rangle |0\rangle_S + |+\rangle |1\rangle_S)}
+ (|+\rangle_S |0-\rangle + |-\rangle_S |1+\rangle) |1\rangle (|+\rangle |0\rangle_S + |-\rangle |1\rangle_S).$$
(10)

Now we perform the fusion operation on qubits 1 and 6 and get

$$\frac{Fusion}{2\sqrt{2}} \left(|10\rangle_{S} \left(|0+0+\rangle + |1-0+\rangle + |0-1-\rangle + |1+1-\rangle \right) + |01\rangle_{S} \left(|0+0-\rangle - |1-0-\rangle + |0-1+\rangle - |1+1+\rangle \right) \right)$$

$$= \frac{1}{2\sqrt{2}} \left(|0\rangle_{L} \left(|0+0+\rangle + |1-0+\rangle + |0-1-\rangle + |1+1-\rangle \right)$$

$$+ |1\rangle_{L} \left(|0+0-\rangle - |1-0-\rangle + |0-1+\rangle - |1+1+\rangle \right) \right).$$
(11)

Here, we have moved the second spin qubit to the first position and reintroduced the logical qubit encoding using $|0\rangle_L$ and $|1\rangle_L$. Additionally, we have added a normalization constant. The expression above represents the state that corresponds to the graph shown in Extended Data Fig. 2,c. The measured stabilizer expectation values are displayed in Extended Data Fig. 2,b.

Tree states

We now describe the experimental protocol for generating the target state of the form

$$|\psi_{tree}\rangle = \frac{1}{2\sqrt{2}} \left(|0\rangle \left(|0++\rangle + |1--\rangle \right)^{\otimes 2} + |1\rangle \left(|0++\rangle - |1--\rangle \right)^{\otimes 2} \right). \tag{12}$$

We start by preparing both atoms in the $|F=2, m_F=0\rangle$ state followed by three sequential photon production cycles on each atom in parallel. From this we obtain the tensor product of two GHZ states, each consisting of one atom and three photons (see also ref. [16]). Omitting normalization constants, we can write the state as

$$|\psi\rangle = (|0\rangle_S |000\rangle + |1\rangle_S |111\rangle) \otimes (|0\rangle_S |000\rangle - |1\rangle_S |111\rangle). \tag{13}$$

Note that the second term carries a relative minus sign with respect to the first term. This is reflected in the parity measurement shown in Fig. 2b of the main text. We now perform a Hadamard gate on all qubits except qubits 2 and 6 (indices run from left to right) and obtain

$$\longrightarrow (|+\rangle_S |0++\rangle + |-\rangle_S |1--\rangle) \otimes (|+\rangle_S |0++\rangle - |-\rangle_S |1--\rangle). \tag{14}$$

For the atoms the Hadamard is carried out with a Raman laser (see main text, Fig. 1e), for the photons it is absorbed into the setting of the measurement basis.

We now merge both branches into one larger graph state by applying the fusion gate. To this end we generate two photons from the atoms with the global STIRAP control laser. Detecting one photon in R and one in L effectively projects the atoms onto the subspace $\{|01\rangle_S, |10\rangle_S\}$.

$$\frac{|01\rangle_{S}\langle01|_{S}+|10\rangle_{S}\langle10|_{S}}{\left(|10\rangle_{S}+|01\rangle_{S}\right)|0++\rangle^{\otimes2}+\left(|10\rangle_{S}-|01\rangle_{S}\right)|0++\rangle|1--\rangle} \\
+\left(|10\rangle_{S}-|01\rangle_{S}\right)|1--\rangle|0++\rangle+\left(|10\rangle_{S}+|01\rangle_{S}\right)|1--\rangle^{\otimes2} \\
=|10\rangle_{S}\left(|0++\rangle+|1--\rangle\right)^{\otimes2}+|01\rangle_{S}\left(|0++\rangle-|1--\rangle\right)^{\otimes2}.$$
(15)

For convenience we have moved the second spin qubit to the first position in the above expression, which allows us to express the two atoms as a logical qubit encoded in the basis $\{|0\rangle_L \equiv |10\rangle_S, |1\rangle_L \equiv |01\rangle_S\}$. Adding a normalization constant we can then write the final state as

$$|\psi_{tree}\rangle = \frac{1}{2\sqrt{2}} \left(|0\rangle_L \left(|0++\rangle + |1--\rangle \right)^{\otimes 2} + |1\rangle_L \left(|0++\rangle - |1--\rangle \right)^{\otimes 2} \right). \tag{16}$$

This is equal to the expression in Eq. 12, with the only difference that the root qubit is now redundantly encoded by the two atoms. Alternatively it would be possible to remove one of the atoms from the state by an X basis measurement.

Coincidence rate

For each multi-qubit state the typical generation and detection rate is between 0.4 and 2.3 coincidences per minute. The total number of events as well as the total measurement time are summarized in Table 1 for each graph state generated in this work. These numbers include all post-selection steps as described above.

Entanglement witness and fidelity lower bound

In order to quantify the agreement between the experimentally produced multi-photon state and the target state, we use an entanglement witness. This has the advantage that we can derive a lower bound of the fidelity without the need for full quantum state tomography. The fidelity of a density matrix ρ with respect to the target state $|\psi\rangle$ is defined as

$$\mathcal{F} = \text{Tr}\{\rho | \psi \rangle \langle \psi | \}. \tag{17}$$

Using the stabilizers we can express the projector to the target state as

$$|\psi\rangle\langle\psi| = \prod_{i} \frac{1+S_{i}}{2} = \prod_{i\in a} \frac{1+S_{i}}{2} \prod_{j\in b} \frac{1+S_{j}}{2} = G_{a} \cdot G_{b}.$$
 (18)

Here we have written the projector as a product of two terms G_a and G_b associated with two sets of stabilizers a and b. Each set a/b can be measured with a single local measurement setting M_a/M_b . These only involve measurements in the X or Z basis for every qubit. We can then write the projector in terms of G_a and G_b giving

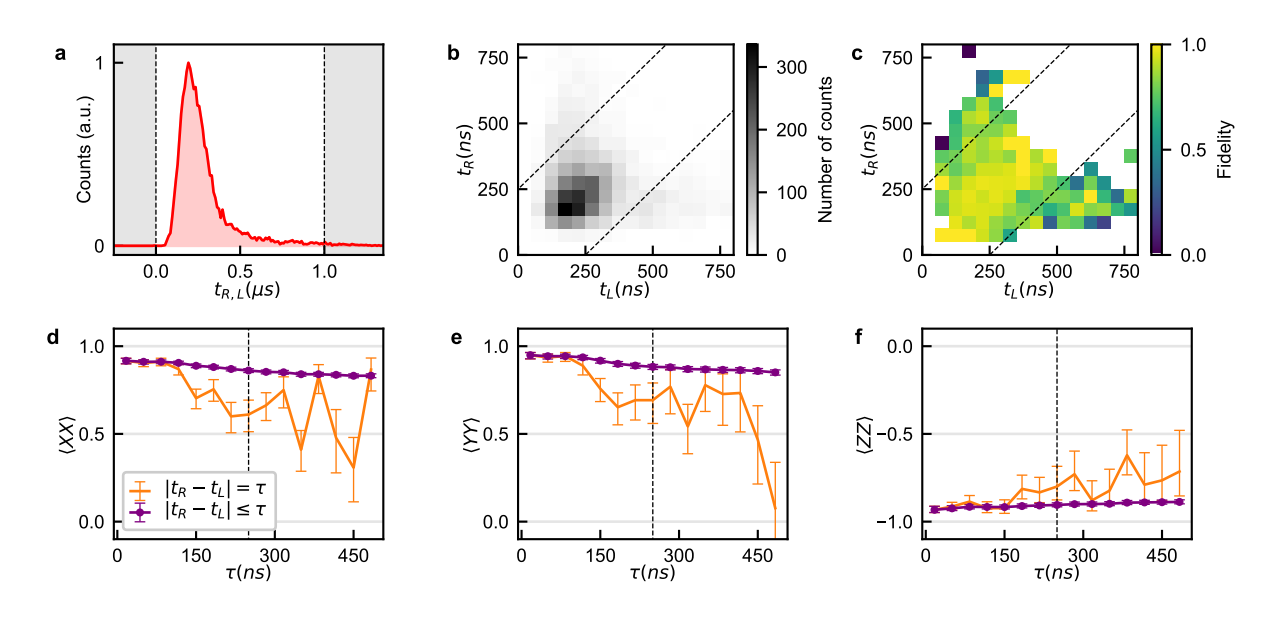
$$|\psi\rangle\langle\psi| = G_a \cdot G_b = G_a + G_b - 1 + (1 - G_a)(1 - G_b)$$
 (19)

As the stabilizers S_i take the values +1 or -1, the product terms G_a and G_b are either 1 or 0. We conclude that $(1-G_a)(1-G_b)$ is non-negative. Omitting this term we find the lower bound

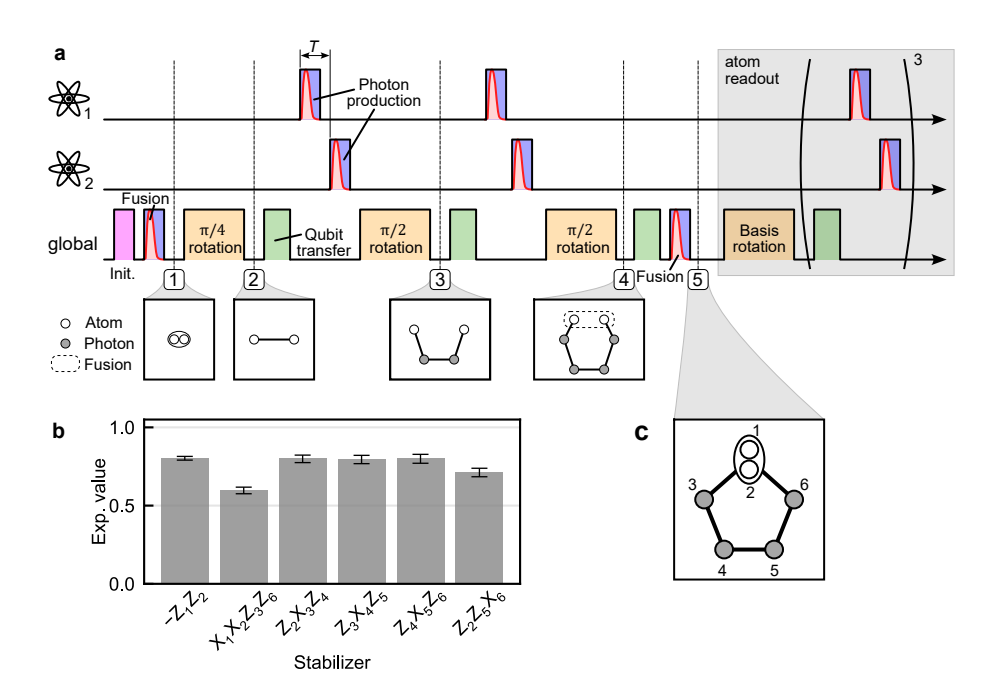
$$P = G_a + G_b - 1. (20)$$

The fidelity \mathcal{F} is then bounded by the inequality $\mathcal{F} \geq \langle P \rangle$. The above expression is applicable if the stabilizers can be divided into two sets a and b, each of which can be measured with a single measurement setting (M_a and M_b). In the context of our experiment, this applies to tree graph states as well as ring graph states of even parity, i.e. an even number of vertices. To the best of our knowledge, there is no equivalent method for ring graph states of odd parity like the pentagon graph, and a fidelity lower bound cannot be derived.

EXTENDED DATA



Extended Data Fig. 1. Atom-atom-entanglement via the cavity-assisted fusion gate. (a) Histogram displaying the total photon count rate as a function of t_R and t_L , where $t_{R/L}$ is the arrival time of the right/left hand polarized photon generated in the fusion process. Only events in which both photons were detected are shown. Dashed lines mark the acceptance window for post-selection. (b) Density plot of the number of counts as a function of t_R and t_L . (c) Density plot of the fidelity as a function of t_R and t_L . (d-f) Expectation values of the correlators XX, YY and ZZ as a function of photon arrival time difference. The orange line displays the correlator for time difference $|t_R - t_L| = \tau$, whereas the purple line is the cumulative correlator, meaning for events where $|t_R - t_L| \le \tau$. The dashed lines mark the maximum τ we choose for Fig. 1c in the main text. Error bars represent the 1σ standard error.



Extended Data Fig. 2. Protocol for the generation of the pentagon graph. A two-atom graph state is obtained from the cavity-assisted fusion gate followed by a $-\pi/4$ pulse. A chain is grown along one dimension using photon emissions and $\pi/2$ rotations on the atomic qubits. Both ends of the chain are merged to form a ring. Error bars represent the 1σ standard error.

	Box	Pentagon	Hexagon	Tree
Number of events	628	392	219	227
Measurement time (h)	4.5	3.3	8.7	4.8
Rate (events/min)	2.3	2.0	0.4	0.8

Extended Data Table 1. Coincidence rate. Coincidence rate statistics for the generated box, pentagon, hexagon and tree graph states.